PAPER

Automatic Data Processing Procedure for Ground Probing Radar

Toru SATO†, Kenya TAKEDA†, Toshio WAKAYAMA†, Iwane KIMURA†, *Members*,
Tomoyuki ABE†† *and* Tetsuya SHINBO††, *Nonmembers*

SUMMARY We developed an automatic data processing algorithm for a ground-probing radar which is essential in analyzing a large amount of data by a non-expert. Its aim is to obtain an optimum result that the conventional technique can give, without the assistance of an experienced operator. The algorithm is general except that it postulates the existence of at least one isolated target in the radar image. The raw images of underground objects are compressed in the vertical and the horizontal directions by using a pulse-compression filter and the aperture synthesis technique, respectively. The test function needed to configure the compression filter is automatically selected from the given image. The sensitivity of the compression filter is adjusted to minimize the magnitude of spurious responses. The propagation velocity needed to perform the aperture synthesis is determined by fitting a hyperbola to the selected echo trace. We verified the algorithm by applying it to the data obtained at two test sites with different magnitude of clutter echoes.

key words: *aperture synthesis, pulse compression, underground detection, automatic data processing, optimization, ground probing radar*

1. Introduction

The ground probing radar technique has been successfully applied for detecting a variety of buried objects. Making the best use of the stationary nature of underground targets, the aperture synthesis (or holographic imaging) technique is an essential tool in the data processing. While it serves to compress the radar image mainly in the horizontal (parallel to the antenna scan) direction, the pulse-compression filter is used to compress the image in the vertical direction.

Although the theoretical aspects of these basic techniques are already established [1], [2], the application to real data has not been straightforward because of various factors such as strong clutter echoes, variability of the pulse waveform due to ground conditions, attenuation, dispersion, and/or inhomogeneity of the propagating medium. In most of practical applications, manual adjustments by an experienced operator have been required to get the optimum image because the image reconstruction techniques assume a homogeneous medium and that targets are in the far field of the antenna, which is often far from the reality.

The object of this paper is to develop a reliable automatic image compression algorithm applicable to the detection of buried objects under the ground of unknown propagation constant and the clutter level so that an unexperienced operator can get a clear image that required the assistance of an expert. We believe that this type of automation is essential in processing a large amount of data by a non-expert.

We first postulate that the medium is locally homogeneous. The homogeneity should apply to the region within which the aperture synthesis for each target point is performed. Although the range varies depending on the attenuation in the medium, the rough measure is given by the horizontal extent of hyperbola in the raw image. We also postulate that each radar image contains at least one isolated target in it. These assumptions certainly limit the applicability of the algorithm, but they are usually satisfied in the practical sense for the case of detecting buried pipes in the ground, which is one of the important fields where the radar technique is very useful.

After briefly reviewing the theory, we examine the performance of the proposed algorithm using real data in the course of presenting its principle. The data sets used here consist of those taken at two test sites with different ground conditions.

2. Principle of Image Reconstruction

The most basic configuration of the underground radar is to scan the transmitting and receiving antennas horizontally together along a baseline. Since the ground and the antenna usually have band-pass characteristics, the received signal suffers appreciable ringing even when a sharp mono-cycle pulse is transmitted. Let us first consider the simplest case where the medium contains only one point target. The deteriorated image can be compressed in the vertical direction by a convolution operation as

$$w(\boldsymbol{x}_{\mathrm{r}}, t) = \int_{-\infty}^{\infty} v_1(\boldsymbol{x}_{\mathrm{r}}, \tau) h_1(t-\tau) \mathrm{d}\tau \ , \qquad (1)$$

where $v_1(\boldsymbol{x}_{\mathrm{r}}, t)$ is the scattered waveform from the point target received at an observation point $\boldsymbol{x}_{\mathrm{r}}$ on the ground,

Manuscript received April 30, 1993.
Manuscript revised September 20, 1993.

†The authors are with the Faculty of Engineering, Kyoto University, Kyoto-shi, 606–01 Japan.
††The authors are with Komatsu Co., Ltd, Hiratsuka-shi, 254 Japan.

$h_1(t)$ is the impulse response of the compression filter, and $w(\boldsymbol{x}_r, t)$ is the compressed waveform. The transfer function of the optimum compression filter given by Osumi and Ueno [1] is expressed as

$$H_1(f) = V_0 \frac{V_1(f)^*}{(1-\eta)V_0^2 + \eta|V_1(f)|^2} , \quad (2)$$

where V_0^2 is its total power of the signal, $V_1(f)$ is the Fourier transform of $v_1(t)$ ($\equiv v_1(\boldsymbol{x}_r, t)$), and f is frequency. Although Osumi and Ueno used an additional filtering term in order to suppress time sidelobes, we get this effect by properly choosing η as discussed later. This expression is equivalent to that of the Wiener filter, and the parameter η should be determined from the signal-to-clutter/noise ratio.

It is thus important to determine the waveform $v_1(t)$ from a single scatterer, which we call 'test function' hereafter, in order to get an accurate form of the compression filter. Actually the form of this test function depends also on the length of propagation because the attenuation is usually frequency dependent. We neglect this effect here, however, since it is not important for shallow targets with similar depth. It should be noted that if $h_1(t)$ is properly determined, the entire image can be compressed using the same filter even when it contains multiple or continuous scatterers.

The horizontal resolution is improved by the aperture synthesis operation, which is expressed for a case of two-dimensional synthesis as [1]

$$b(\boldsymbol{x}) = \int_{-\infty}^{\infty} w(\boldsymbol{x}_r, 2|\boldsymbol{x} - \boldsymbol{x}_r|/c_u) \frac{z^3}{|\boldsymbol{x} - \boldsymbol{x}_r|^3} \mathrm{d}x_r , \quad (3)$$

where c_u is the speed of light in the medium, and $b(\boldsymbol{x})$ is the compressed image at a point $\boldsymbol{x}$. The x and z axes are taken to be the horizontal and the vertical directions, respectively.

As a summary, the parameters to be determined are η, the test function $v_1(t)$, and c_u. We will discuss practical procedures to estimate these parameters from a given set of data in details in a later section.

3. Test Data

In order to examine the performance of our algorithm under practical conditions, we applied it to two data sets taken under different medium conditions using the same radar system developed by Komatsu Co., Ltd. [3]. The radar system transmits a mono-cycle pulse of 3-nsec width at an interval of 6 μsec. The transmitting and receiving antennas are bow-tie antennas of the same size, located side-by-side with a separation of 0.4 m in a chassis of 0.64 × 0.64 m. The received signal is sampled at 256 range bins with 0.25 nsec sampling interval with an 8-bit A/D converter, and thereafter averaged for 64 pulse-cycles. The data is then stored in a micro computer for off-line processing. The scanning is made manually, and the position is measured by recording the rotation of wheels attached to the chassis.

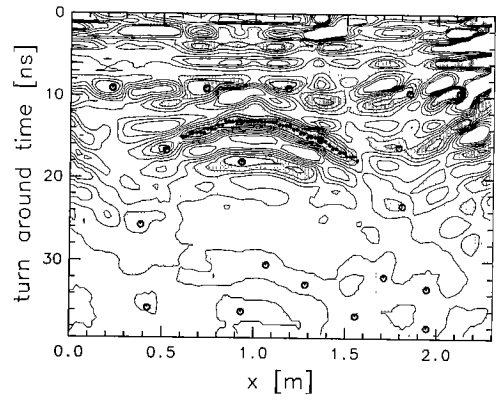

Fig. 1 Original cross-sectional image of Test Data 1. Small circles indicate local maxima, and the small triangle indicates the maximum of the curve which best fits a hyperbola as shown by dots.

Test Data 1 is taken at an in-house test site filled with dry sand. Dimensions of the site are $x = 3.34$ m, $y \sim 10$ m, $z = 2.00$ m. An aluminum pipe of length 1.55 m and diameter of 3 cm is buried at $z = 1.05$ m aligned to y-axis, and the radar scanned along x-axis above the center of the pipe. The horizontal sampling interval is 2 cm. It should be noted that test site 1 was made by digging trenches to lay pipes. Figure 1 shows an example of the original cross-sectional image of Test Data 1 after subtraction of the mean signal level at each depth. The image shown here is a part of the original record, and consists of 160 × 115 sample points in the time and the horizontal axis, respectively. The contours indicate the electric field strength of the received signal at an arbitrary scale. White and the darkest shading corresponds to the negative and the positive maximum voltage, respectively, of the A/D converter. The symbols in the figure are explained later in the algorithm section. This data represents a rather idealized situation of a fairly uniform medium with relatively small amount of clutter echoes. Peaks at around 10 nsec are due to variations of the waveform of the ground-surface echo caused by slight variations in the antenna height above ground while scanning was made. It was confirmed by checking the ground echo pattern versus the antenna height above the ground, and attributed to a poor impedance matching of the antenna with the ground.

Test Data 2 represents a more realistic situation. It is taken at a test site in an open urban area with buried pipes of known shape, material, and location. Figure 2 shows schematically its cross section and plane view. The ground condition is typical for the ground under a road in a city area with heavy traffic. The structure of the pavement from the surface is: 5-cm fine asphalt layer, 30-cm coarse asphalt layer, 15-cm fine macadam layer, 20-cm coarse macadam layer. The soil under the

pavement is moist sand. Although the precise water content of the sand is not known, the mass ratio of water to the total mass is estimated from the speed of light to be about 10 %. Targets are iron-reinforced concrete pipes of length 3 m and diameter 30 cm, partly covered by shorter pipes of the same material but with length 1 m and diameter 60 cm. The data is taken by a scan across three such pipes buried at a depth of 1.5 m as shown in the figure. The horizontal sampling interval is 8 cm. Figure 3 shows the original image of Test Data 2. It consists of 256 × 86 sample points. The layered echoes at 7 nsec and 15 nsec are caused by interfaces between different layers of the pavement, and that at 22 nsec seems to be due to ringing of such echoes.

Although only one image for each two data sets will be shown in the following sections for consistency, we obtained several images for each data set with slightly different ground conditions, path of the scan, and configurations of targets. The algorithm described here was applied to all of these images without changing internal parameters manually, and was confirmed to give similar performances for all cases.

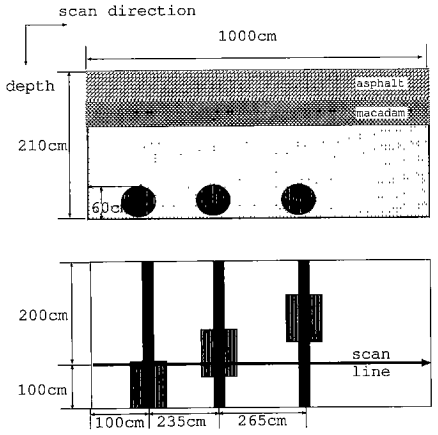

Fig. 2 Schematic cross section (top panel) and plan view (bottom panel) of the site for Test Data 2. The scan line is indicated by a thick line in the bottom panel.

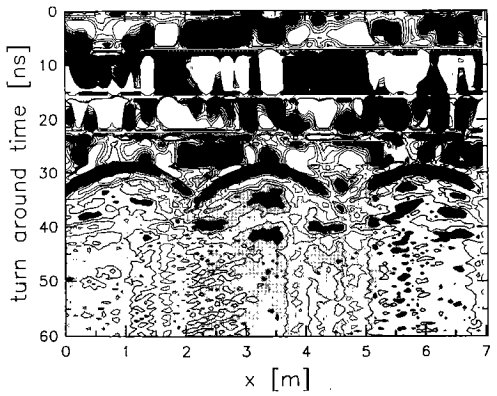

Fig. 3 Original image of Test Data 2.

4. The Algorithm

The automatic data processing algorithm proposed here consists of three steps. First an isolated target is searched by finding a curve which resembles a hyperbola. The time response on such curve is used as the test function $v_1(t)$. Second, the optimum parameter η for the compression filter is determined from $v_1(t)$. Finally, the optimum value of c_u for the aperture synthesis is determined.

4.1 Selection of the Test Function

As shown before, we have to choose a proper test function $v_1(t)$ in order to get the optimum vertical compression. While it is possible to measure the impulse response of the system including the antenna, it is not feasible to directly measure that of the propagation medium. The most practical solution for this problem is to find an echo from an isolated point target in the given raw image data, and use its waveform as $v_1(t)$. If such an echo exists in the image, it appears as a clear hyperbola in the $x-z$ plane. Here we develop a practical method of selecting a curve which best fits a hyperbola in the given image data.

The first step of this procedure is to find local maxima. A local maximum is defined as a point that gives the maximum signal intensity in the grid of 7 × 7 sample points (1.75 nsec × 14 cm in Fig. 1) centered at that point. These maxima are indicated by small circles in Fig. 1. Those points with the time delay of less than 6 nsec are not counted even when they satisfy this condition, because they may be affected by the echo from the ground surface.

From each of these local maxima, whose position is (x_{i0}, z_{j0}), we then try to extend a curve in the x-direction by connecting the maximum points in the z-direction at given x. From a curve point (x_i, z_j), the next curve point at x_{i+1} is determined as a point that has maximum signal intensity in the range from (x_{i+1}, z_{j-5}) to (x_{i+1}, z_{j+10}). The extension of the curve is terminated when the signal intensity on the curve becomes less than half of that at (x_{i0}, z_{j0}). The curve is also extended to negative x-direction in the same manner. For each curve which consists of N points, a hyperbola is fitted in a least-squares sense. If c_u determined from the best-fit hyperbola has an unrealistic value (negative, or larger than free space), the curve is not considered for further analysis.

Finally, we compare 'badness' b of the curves as defined by

$$b = \sum_i (z_j - z_{\text{fit}})^2 / N^3 , \tag{4}$$

where z_{fit} is the position of the best fit hyperbola at x_i. The expression for b was chosen empirically to give

a small badness for a curve that has a long horizontal extension and also has a good fit to a hyperbola.

The small triangle in Fig. 1 indicates the local maximum that has the curve with smallest badness in the entire image. The curve points are indicated by dots, and the best fit hyperbola is shown by a thin curve.

The test function $v(t)$ is given by the time response on this selected curve. In order to suppress clutter echoes, the time response is averaged over the entire curve, adjusting the z value according to $z_{\rm fit}$ as

$$v_1(z_j) = \sum_i v(x_i, z_j + z_{\rm fit})/N \ . \tag{5}$$

This operation is equivalent to the migration stack technique commonly used for the seismic data processing [4]. The dot-dashed curve in the left panel of Fig. 4 shows the signal waveform thus determined.

It should be noted here that we have not yet determined the actual time delay where the echo starts. What we have determined is $v_1(t-t_0)$ with unknown t_0. The next step is to determine this value. If the received waveform was not contaminated by clutter echoes, it is a straight forward task, because we only need to find the wave front (time delay where non-zero value first appears). However, as shown in this waveform, the wave front of the echo is not yet clear because it is masked by the clutter echoes from ground layers. The magnitude of the clutter echoes in the raw recieved signal is a few order larger than the desired echoes from the pipe. Although these clutter echoes are mostly suppressed by removing the x-mean values at each z point, the remaining parts of the clutter are still strong enough to contaminate the signal.

In order to remove these contamination, variance $\sigma(z_j)$ among the N waveforms normalized by $v_1(z_j)^2$ is computed at each z_j value.

$$\sigma(z_j) = \frac{1}{N}\sum_i \left\{ \frac{v(x_i, z_j + z_{\rm fit}) - v_1(z_j)}{v_1(z_j)} \right\}^2 \tag{6}$$

This normalized variance should be larger than 1 where contamination prevails, and should have a minimum where the relative amplitude of v_1 against the contamination takes its maximum value. We should note that the largest peak of σ itself does not necessarily coincide with the peak of signal v_1 because the magnitude of the contamination rapidly decreases as the depth increases. The right panel shows the ratio of σ averaged for 5 points above and below the current z value. The peak of this curve thus indicates a point above which the variance is largest relative to that below. It is expected that this peak coincides with the first peak of the real echo from the target. We found from experiments with known location of the pipes that the real wave front is located about 2 nsec (8 points) above the peak of this curve. This value is determined from the response (or correlation) time of the original mono-cycle pulse. Arrows in Fig. 4 shows the wave front thus determined. The contamination in the test function is removed by attenuating the signal above this wave front as shown by the thick curve in the left panel.

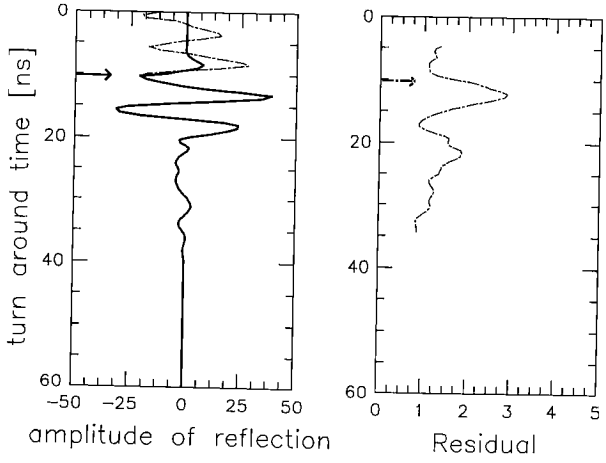

Fig. 4 The waveform of the selected test function from Fig. 1 (left panel), and the residual used to determine the wave front (right panel). The dot-dashed curve and the solid curve in the left panel are the waveform before and after suppression of the echoes from ground layers, respectively. The arrows indicate the estimated wave front.

4.2 Optimum Pulse Compression

In the pulse compression filter shown in Eq. (2), we neglected an additional filter term which was used in the original reference to suppress the time sidelobes of $w(t)$ at specified time points. Instead we employ a simpler alternative of choosing the parameter η that gives the minimum sidelobe responses. In this way, we can handle the optimization of the compression filter by a single parameter.

We define the magnitude of the time sidelobe S_g as

$$S_g = \sum_{|j|>\epsilon} w(z_j)^2 \ , \tag{7}$$

where ϵ is the half-width of the 'main lobe'. Here we use $\epsilon = 20$ (5 nsec). Figure 5 shows the variation of S_g

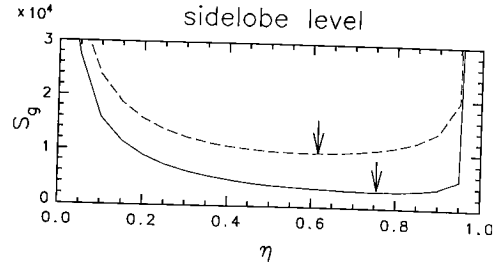

Fig. 5 Variation of time sidelobe level S_g versus the parameter η of the compression filter. The solid curve and the dashed curve is for Test Data 1 and 2, respectively. The arrows indicate the optimum η.

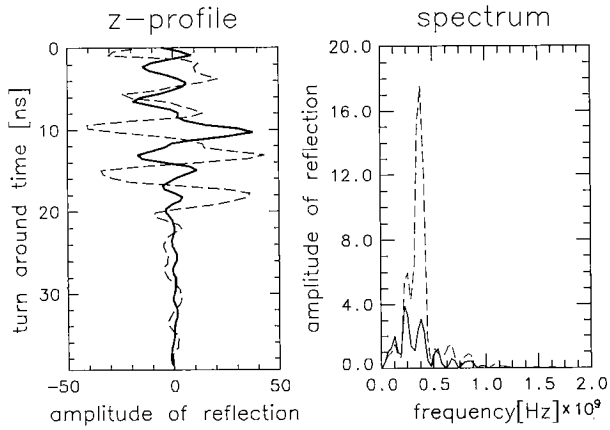

Fig. 6 Uncompressed (dashed curve) and compressed (solid curve) waveform of Test Data 1 using the optimum parameter $\eta = 0.75$ (leftpanel), and their power spectrum (right panel).

computed for η of 0–1 for Test Data 1 (solid curve) and 2 (dashed curve). The compression filter approaches to the inverse filter as η increases, and to the matched filter as η decreases. The difference between these two curves clearly shows the difference of the clutter level of the two test data sets. Test Data 1 takes a small minimum value of S_g at $\eta = 0.75$, while Test Data 2 has a larger minimum at $\eta = 0.62$. The shallow minimum in this figure is mainly due to the existence of clutter contaminations, which raise the bottom level of S_g. The obtained image largely deteriorates when we change η by plus or minus 0.1 from the optimum value.

It is thus possible to automatically choose an appropriate form of the compression filter according to the quality of data. Figure 6 shows the uncompressed (dashed curve) and compressed (solid curve) waveforms of Test Data 1 (left panel), and their Power spectrum (right panel).

4.3 Optimum Aperture Synthesis

Horizontal compression of the image is performed by the aperture synthesis operation of Eq. (3). An important factor to be determined here is the speed of light c_u in the medium. Here we postulate that the medium is locally uniform, so that the aperture synthesis operation can be performed assuming c_u is constant.

We can determine c_u by fitting a hyperbola to the curve of the echo from an isolated target as described above. The equation for the curve is given by

$$\{(t/2)^2 - (t_0/2)^2\}\, c_u^2 = (x^2 - x_0)^2 \,, \tag{8}$$

where t_0 is the round-trip time of the echo from a target when the radar observes from above the target located at x_0. We determine c_u by fitting this equation to the observed curve. This equation is linear in terms of t^2, so that the optimum value of c_u can be determined using the linear least-squares fitting procedure. Figure 7

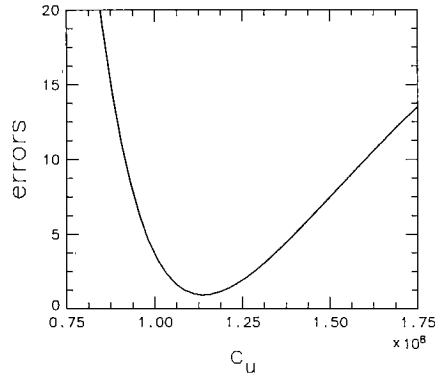

Fig. 7 Square error of t^2 between the hyperbola and the observed curve of echo as a function of the speed of light c_u.

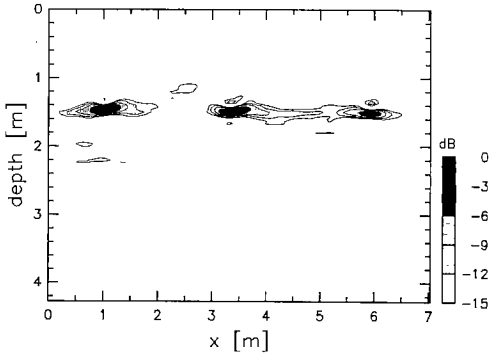

Fig. 8 Compressed radar image of Test Data 2 after the aperture synthesis.

shows the sum-of-squares error versus c_u for the purpose of demonstration for Test Data 1.

After determining the optimum c_u, the compressed radar image is obtained by applying Eq. (3) to the image after the pulse compression discussed in the previous section. For Test Data 1, which contains only one single target in the entire image, the final image is almost perfectly compressed to a delta function with only weak remainder of clutter echoes. It is not surprising, however, since both the pulse compression and the aperture synthesis was performed using the echo from the target itself as the test function.

Figure 8 shows the result for Test Data 2. The program chose the echo from the pipe at the center as the test function, and the entire image was compressed using the same test function, η, and c_u. As can be seen in the figure, all three pipes are clearly identified with only slight remainders of the clutter echoes. It should be noted that all other images of Test Data 2 taken under similar ground conditions and target configurations at the same test site showed similar quality of compression.

5. Discussion

We examined the proposed automated signal processing algorithm using two test data sets taken under different

ground conditions. It has been found that the algorithm works properly without any manual adjustments if the image contains at least one isolated point target in it.

Although the test data shown here contains only point targets, the algorithm is expected to work for the case that also contains continuous targets, as far as the effect of multiple scattering is not serious.

The current algorithm finds only one curve with the minimum badness in determining the test function since the length of scan was limited. If a much longer scan is to be processed at a time, the algorithm can be fairly easily extended to take more curves with allowable badness in the image in order to adapt for a smooth variation of the propagation constant in the medium.

Another limitation of the current algorithm is that it neglects the dependence of the test function on the length of propagation. It is not a problem for the case of shallow targets with similar depth as examined here, but it should be considered when the targets have a wide variety of depth. Turner [5] developed a deconvolution technique that takes the dispersion and the frequency selective attenuation into account in constructing the inverse filter. The same technique can be introduced into the current algorithm if the data contains two or more isolated targets with sufficiently different depth.

In the present program, the aperture synthesis operation is applied to the entire image without any effort of reducing the computation time, such as the preprocessing technique which limits the region of the synthesis operation [6]. Although it has been said that the full aperture synthesis is time consuming, the entire processing of our algorithm was performed in about 50 sec for the examples shown here using a SUN SPARC station 2. Since the combination of a microcomputer and a digital-signal-processing board often provides a much faster speed than such a general-purpose workstation, the computation time may not be a serious limitation any more for some applications like the present case. Future extensions of the study on data processing should consider the applicability of the algorithm for a more general situation as well as to consider the processing speed.

References

[1] Osumi, N. and Ueno, K., "Microwave Holographic Imaging method with Improved Resolution," *IEEE Trans. Antennas and Propagation*, vol.32, no.10, pp.1018–1026, Oct. 1984.

[2] Osumi, N. and Ueno, K., "Detection of buried plant," *IEE Proc.*, vol.135, no.4, pp.330–342, Apr. 1988.

[3] Suzuki, T. and Arai, I., "Advance on underground radars," *IEICE Trans.*, vol.E74, no.2, pp.289–293, Feb. 1991.

[4] Gazdag, J. and Sguazzero, P., "Migration of seismic data," *Proc. IEEE*, vol.72, no.10, pp.1302–1315, Oct. 1984.

[5] Turner, G., "Propagation deconvolution," *Fourth Int. Conf. Ground Penetrating Radar*, pp.85–93, Jun. 1992.

[6] Michiguchi, Y., Hiramoto, K., Nishi, M., Takahashi, F., Ohtaka, T. and Okada, M., "Development of signal processing methods for imaging buried pipes," *IEEE Trans. Geosci. Remote Sensing*, vol.GE-25, no.1, pp.11–15, Jan. 1987.

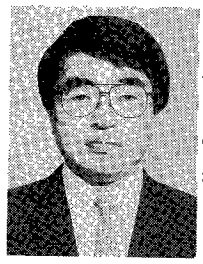

Toru Sato received the B.E., M.E., and Ph.D. degrees in electrical engineering from Kyoto University, Kyoto, Japan in 1976, 1978, and 1982, respectively. He was a graduate student research associate of Arecibo Observatory, National Astronomy and Ionosphere Center from 1979 to 1980. He joined Radio Atmospheric Science Center of Kyoto University in 1983 as a research associate. He moved back to Department of Electrical Engineering II, Kyoto University in 1988 as a lecturer, and is now an associate professor. His research interests have been radar remote sensing of the atmosphere, observations of precipitation using radar and satellite signals, radar observation of space debris, signal processing for subsurface radars, and digital satellite communication. He was awarded Tanakadate Prize in 1986. He is a member of the Society of Geomagnetism and Earth, Planetary and Space Sciences, the Japan Society for Aeronautical and Space Sciences, the Institute of Electrical and Electronics Engineers, and American Meteorological Society.

Kenya Takeda received the B.E. degree in electrical engineering from Kyoto University, Japan in 1992. He is currently working toward M.E. degree at Department of Electrical Enginnering II, Kyoto University. His research interest is radar image reconstruction.

Toshio Wakayama received the B.E. and M.E. degrees in electrical engineering from Kyoto University, Japan in 1990 and 1992, respectively. He is currently working toward Ph.D. degree at Department of Electrical Enginnering II, Kyoto University. His research interest is signal processing for subsurface radars.

Iwane Kimura received the B.E., M.E., and Ph.D. degrees in electrical engineering from Kyoto University, Kyoto, Japan in 1955, 1957, and 1961 respectively. Since 1960, he has been a staff of Kyoto University; Department of Electronics and Department of Electrical Engineering II where he is now a Professor radio engineering since 1971. He has also been a visiting Professor of Institute of Space and Astronautical Science from 1981 to 1991. From 1964 to 1965, he was a research associate at Radioscience Laboratory, Stanford University on leave from Kyoto University. His research interests have been in radio science; particularly remote-sensing of upper atmospheres by radar techniques, and space plasma physics, such as theoretical study on propagation and generation of radio waves in magnetospheric and ionospheric plasmas, plasma measurements by rocket-Doppler technique, and active wave experiments in space plasmas using scientific satellites. He was awarded Inada Memorial Prize in 1958, and Tanakadate Prize in 1961. He is a member of the Institute of Electrical Engineers of Japan, the Society of Geomagnetism and Earth, Planetary and Space Sciences, and the American Geophysical Union.

Tomoyuki Abe received the B.E. degree from Osaka University in 1973. He joined Komatsu Co., Ltd. in 1980, where he was engaged in the study of heat pump at Research Institute, and in the development of underground radars and void detectors for tunneling machines at Electronic Research Institute, respectively. He is now the head of the planning division of Komatsu House Co., Ltd. He is a member of Japan Society of Geoinformatics.

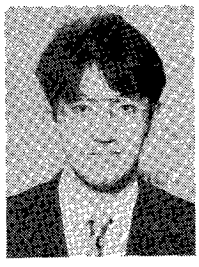

Tetsuya Shinbo received the B.E. and M.E. degrees in electrical engineering from Kanazawa University, Japan in 1985 and 1987, respectively. He joined Komatsu Co., Ltd. in 1987. His research interest is detection of underground objects using radio wave. He is also working now for the Ph.D. degree at Department of Electrical Engineering, Kanazawa University.